



This is a repository copy of *Impact of aromatic structures and content in formulated fuel for jet engine applications on particulate matter emissions*.

White Rose Research Online URL for this paper:
<https://eprints.whiterose.ac.uk/172506/>

Version: Accepted Version

Article:

Zheng, L., Singh, P., Cronly, J. et al. (5 more authors) (2021) Impact of aromatic structures and content in formulated fuel for jet engine applications on particulate matter emissions. *Journal of Energy Resources Technology*, 143 (12). 122301. ISSN 0195-0738

<https://doi.org/10.1115/1.4049905>

© 2021 by ASME. This is an author-produced version of a paper subsequently published in *J. Energy Resour. Technol.* Article available under the terms of the Creative Commons Attribution Licence (<http://creativecommons.org/licenses/by/4.0>).

Reuse

This article is distributed under the terms of the Creative Commons Attribution (CC BY) licence. This licence allows you to distribute, remix, tweak, and build upon the work, even commercially, as long as you credit the authors for the original work. More information and the full terms of the licence here:
<https://creativecommons.org/licenses/>

Takedown

If you consider content in White Rose Research Online to be in breach of UK law, please notify us by emailing eprints@whiterose.ac.uk including the URL of the record and the reason for the withdrawal request.



eprints@whiterose.ac.uk
<https://eprints.whiterose.ac.uk/>



ASME Accepted Manuscript Repository

Institutional Repository Cover Sheet

Zhang

Y.

First

Last

ASME Paper Title: Impact of aromatic structures and content in formulated fuel for jet engine applications on parti
matter emissions

Authors: Lukai Zheng , Paramvir Singh , James Cronly , Emamode A. Ubogu , Ihab Ahmed , Chenxing Ling , Yang
Zhang , Bhupendra Khandelwal

ASME Journal Title: J. Energy Resour. Technol.

Volume/Issue 143 (12) Date of Publication (VOR* Online) 22/02/2021

ASME Digital Collection URL: <https://asmedigitalcollection.asme.org/energyresources/article-abstract/143/12/122301/1096794/Impact-of-Aromatic-Structures-and-Content-in?redirectedFrom=fulltext>

DOI: <https://doi.org/10.1115/1.4049905>

*VOR (version of record)



This is a repository copy of *Impact of Aromatic Structures and Content in Formulated Fuel for Jet Engine Applications on Particulate Matter Emissions*.

White Rose Research Online URL for this paper:
<http://eprints.whiterose.ac.uk/172506/>

Version: Accepted Version

Article:

Zheng, L, Singh, P, Cronly, J et al. (5 more authors) (2021) Impact of Aromatic Structures and Content in Formulated Fuel for Jet Engine Applications on Particulate Matter Emissions. *Journal of Energy Resources Technology, Transactions of the ASME*, 143 (12). ISSN 0195-0738 (In Press)

<https://doi.org/10.1115/1.4049905>

Reuse

Items deposited in White Rose Research Online are protected by copyright, with all rights reserved unless indicated otherwise. They may be downloaded and/or printed for private study, or other acts as permitted by national copyright laws. The publisher or other rights holders may allow further reproduction and re-use of the full text version. This is indicated by the licence information on the White Rose Research Online record for the item.

Takedown

If you consider content in White Rose Research Online to be in breach of UK law, please notify us by emailing eprints@whiterose.ac.uk including the URL of the record and the reason for the withdrawal request.



eprints@whiterose.ac.uk
<https://eprints.whiterose.ac.uk/>

Impact of aromatic structures and content in formulated fuel for jet engine applications on particulate matter emissions

Lukai Zheng

Department of Mechanical Engineering,
Nanjing institute of technology,
Nanjing, Jiangsu, 211167, China
e-mail: lukaizheng7@gmail.com

Paramvir Singh

Combustion Research Laboratory,
Indian Institute of Technology Bombay,
Powai, Mumbai 400 076, India
e-mail: param016@gmail.com

James Cronly

Low Carbon Combustion Centre
University of Sheffield,
Sheffield, S20 1AH, United Kingdom
e-mail: jcronly1@sheffield.ac.uk

Emamode A Ubogu

Low Carbon Combustion Centre
University of Sheffield,
Sheffield, S20 1AH, United Kingdom
e-mail: seriesfure@gmail.com

Ihab Ahmed

Low Carbon Combustion Centre
University of Sheffield,
Sheffield, S20 1AH, United Kingdom
e-mail: i.s.ahmed@sheffield.ac.uk

Chenxing Ling

Low Carbon Combustion Centre
University of Sheffield,
Sheffield, S20 1AH, United Kingdom
e-mail: cling3@sheffield.ac.uk

Yang Zhang

Low Carbon Combustion Centre
University of Sheffield,
Sheffield, S20 1AH, United Kingdom
e-mail: yz100@sheffield.ac.uk

Bhupendra Khandelwal¹

Department of Mechanical Engineering,
University of Alabama,
Tuscaloosa, AL 35487, USA
e-mail: bhupendra.khandelwal@gmail.com

ABSTRACT

Fuel formulation with the particular selection of fuel components is a promising approach that offers the reduction of harmful emissions without altering the combustion system performance. Each fuel component has its own combustion characteristics and hence contribution to emissions. Aromatic is one of the main components of fossil based fuels and has a strong correlation with the formation of PM emissions. Besides, aromatics presence in fuel is essential for the compatibility of fuel with the combustion system and maintaining the energy density of the fuel. In this regard, a Rolls Royce combustor rig was used to test 16 aromatics blended with jet fuels in three different proportions. Moreover, a novel approach of flame luminosity imaging is employed to measure the PM emissions through the soot propensity profile. The results show that PM emissions increase with the proportional increase of aromatics. The di- and cyclo-aromatics produced significantly higher PM emissions compared to alkyl-benzenes. 3-isopropylcumene tends to lowest PM formation and thus is a consideration as a selection of aromatic type in future fuels for lower PM emissions. Furthermore, it was also observed that PM number concentration measured by the extractive method with DMS500 instrument correlates well with imaging methods for all the tested fuels. The present study provides information on particular selection of aromatic for future fuel development.

Keywords: Aromatics; Flame luminosity imaging; PM Emissions; Soot; Tay Combustor

¹ Corresponding author: B. Khandelwal, Associate Professor, Mechanical Engineering Department, University of Alabama Tuscaloosa, AL 35487, USA

INTRODUCTION

For supply security and environmental sustainability, alternative fuels and drop-in fuels for jet engines are of significant importance in energy research. The criteria of high reliability and stabilization of the combustion processes and ignition time have been strictly followed for the potential fuel feedstock [1, 2]. The present human behavior towards industrialization promotes global warming and accelerates climate change [5]. The restrictions of the environmental protection agencies have forced the fuel companies to focus on low emissions as one of the top priorities. Additionally, particulate matter (PM) is of concern to air-quality and profoundly affects the health and environment.

PM emission from different jet fuels from fuel combustion has various concentration levels, particle size, density, and shape under the same operation condition [3, 4]. The formation of free radicals, oxidation of fuels, appended structure of complex aromatics, etc., promotes the soot formation during fuel combustion [6-8]. The aromatic part in fuel composition is a primary cause for the formation of PM or smoke [9].

Alternative fuel has been focused on due to the cost and emission problem for conventional jet fuel. Roughly, alternative fuels could be divided into two categories depending on their feedstock. The Fischer-Tropsch (FT) process is the most mature alternative fuel production pathway to produce synthetic fuels from fossil feedstock like natural gas and coal. Recently, synthetic fuels with FT processes have used bio-based feedstock and have massive potential in the near future. Other alternative fuels use bio-feedstock, such as animal fat, oilseeds, waste oils. As time passed, more feedstock is discovered, which can be converted into jet fuel. Benefit from these formulated fuels and

production pathways; the industries are now able to produce aviation fuels that comprise small amounts of aromatics [10-12], e.g., synthetic paraffinic kerosene, FT derived fuels, gas-to-liquid, etc. The aromatics in fuels are responsible for fuel compatibility with the fuel system, better tribological performance of fuels, and higher energy density per unit mass [13, 14]. Thereby, those alternative fuels could cause fuel leaking and are not suitable for direct use in current commercial flights [15]. ASTM D7566 [16] stipulates that FT SPK's blending ratio should be up to 50/50 by volume and 30/70 for alcohol to jet (ATJ). The minimum aromatic content of 8% has been adopted for synthetically-produced fuels and requires blending with conventional fuels or synthetic aromatics. All the aromatics have a different tendency to promote the formation of pollutant emissions [17]. Thus, the proper selection of synthetic aromatics provides optimization in terms of emission and operability. The choice of promising aromatic would be beneficial for future fuel formulation.

Soot consists of particles with different physical (non-uniform shapes of varying sizes) and chemical properties [18-20]. At the end of the flame plume, the bright yellow sooty flame is due to the heated soot particles during the fuel combustion [21-23]. Numerous expensive and complicated diagnostic systems have been employed to monitor the emissions rate in real-time. The authors in literature have employed a flame luminosity visualization approach to depicting the soot detection and combustion process [25-28]. The research teams of Jiotode [29] and Fujino [30] have experimentally estimated the combustion efficiency and flame temperature distribution by time-resolved imaging data through a visualization approach in the combustion chamber. The paraffin's effect

on soot tendency was investigated by the soot particle mass correlation with soot flame height [31]. Botero [32] also investigated the effect of aromatic contents on soot particle formation with particle size number and luminous temperature. Witkowski [33] have utilized transmission electron microscope (TEM) imaging to propose the diffusion flame soot propensity model by linking the soot profile and LII (Laser-Induced Incandescence). Huang and Zhang [34, 35] proposed digital flame color discrimination (DFCD). The flame colors can be used for the condition of the instantaneous flame mixture through this approach. An alternative non-intrusive approach can monitor the immediate soot formation behavior through imaging post-processing and optical detection method for liquid fuel combustion [36, 37]. A well-known instrument, DMS 500, was used to quantify PM concentration over the full particle size spectrum and real-time size distribution information [38, 39]. Condensation particle counter (CPC) quantified PM number concentration are in good consistency with DMS 500 [40, 24].

From the above discussion, it can be observed that knowledge on the impact of different types of aromatic species in jet fuel would help the industry to take steps forward for future fuels. This study investigates how different aromatics species and their proportions in jet fuel impact PM emissions in a gas turbine combustor. DMS500, alongside the optical combustion monitoring method, was used in this study. The high-speed imaging technique imparts new insight into the soot formation tendencies at extremely stable and lean burning conditions for the aromatic blended fuels. This investigation will help in optimizing current fuel design and future revolutions in the field of energy.

EXPERIMENTAL SPECIFICATION

Test Fuels

For jet fuel use today, the aromatic contents are in the range of 8% to 25%, which can be adopted for synthetically-produced jet fuel. Different types of aromatics produce different levels of smoke and emissions. In this experimental investigation, 16 aromatics species were blended with a base blend comprising a C10-C13 straight-chain hydrocarbon solvent in proportions of 8%, 13%, and 18%. They were evaluated regarding their performance related to PM concentration number and sooty flame formation. The aromatics species structures and properties details are provided in Table 1.

According to aromatics' chemical structures, all tested aromatic species were grouped into three types, namely, alkyl-benzenes, di-aromatics, and cyclo-aromatics, as tabulated in Table 1, [41]. In the Alkyl-benzenes group, one or more hydrogen atoms of the benzene are replaced by alkyl groups of different sizes. For cyclo-aromatics, the series of atoms replace more than one hydrogen atom and are connected to form a ring. The di-aromatic comprise a fused benzene ring pair. Among them, tetrahydronaphthalene is the partially hydrogenated derivative of naphthalene hydrocracking.

Test Conditions

Rolls-Royce Tay combustor was used for the experimentation [42]. The detailed experimental setup is schematically provided in Fig. 1. Airblast atomizer coupled with the combustor. The air was supplied to the combustor by process line through the atmospheric pressure fan and designed as per the industrial design standard (BS:5167). The inlet temperature is up to 775K. The inlet temperature was increased to 775K using

an electric heater; the heater has an automatic feedback loop to maintain the desired temperature. The uncertainty in the measurement of mass flow rate is $\pm 2\%$. A speed controller is employed to control fan drive motor and atmospheric pressure through LabVIEW code execution. The speed controller of the fan was controlled by a labview code, which acts with a feedback loop and takes input in form of mass flow rate required. Calibrated orifice plate based mass flow controllers are used to provide the mass flow rate information to the labview code.

An electronically controlled fuel system was employed to supply the fuel to the combustor. The fuel pressure of 300 kPa was supplied through a nitrogen cylinder and maintained by a regulated valve. A two staged calibrated pressure regulator regulated the pressure to ensure that no operating conditions change during the tests. A twin series (fine and coarse) of air-actuated needle valves and an air-actuated fuel shut-off solenoid were employed to control the exiting fuel—the LV analog voltage controller (5 Hz) through the control system. NI SCXI chassis were used to manage the air-actuated fuel control values and air-fan motor speed controller. The Coriolis meter and orifice flow meter readings are displayed on the system's screen and used to monitor the fuel flow and atmospheric pressure airline, respectively.

The formulated fuels were tested using two operation conditions i.e., stable and lean blow-out (LBO). The details of the gas turbine testing parameters are tabulated in Table 2.

The flow of fuel was maintained at 1.8g/s at the stable burning condition of fuels. All the other testing conditions were maintained after reaching the combustor to steady-

state for LBO detection. The flow rate decreases by LabView code to 0.0001 g/s for the last 0.2g/s until flame blow-out prevailed. The exhaust gas temperature and pressure upstream of combustors were found to have an instant reduction that identified the blow-out. Five consistent points were taken to repeat the above procedure once the LBO point was prevailed [43].

PM Emission Measurements

A sample line was used to deliver the soot particles from the exhaust vent to the analyzer. The particles gain charges in the exhaust sample line via a corona discharge charger; afterward, particles were moved to the classifier. The charged particles were then diverted toward the electrometer rings through high voltage central electrode application. The electrometer ring nearer to the inlet of the sample attracts the higher charged/lower dragged particles. Consequently, the charge of particles flows to the ground through the electrometer amplifier. The small currents generated by these particles in-group is the base of particle quantification. For each size bin, number-weighted particle mobility diameter (D_p) distribution average, $n(D_p) = dN/d\log D_p$, was recorded. The particle size distribution was created by using this distribution and then integrated to generate the total number concentration per volume of the exhaust. Each experiment was repeated thrice to ensure accuracy in the measured values.

Sooty Flame Morphology

The sooty flame analysis was done with a Photron-SA4 high-speed color camera. A quartz window was provided on the exhaust duct in the axial direction to the combustor

chamber for optical access to the burner. The images of the flame plume were taken at the tail through the exhaust vent. For LBO imaging, the shutter speed was set as 1/1000s to capture both the bright yellow flame and the dim blue chemiluminescence because a longer exposure time can avoid the drop-out of weak blue signals [44]. The camera was employed with the end trigger mode and fixed to record continuously till the trigger was pressed at the blow-out point. After that, imaging data of the flame at two seconds (2000 images) before that point was saved. All the attained imaging data were quantitatively analyzed using MatLab image-processing, and adjusted the sample flame pictures shown in this paper via the DFSC approach for better flame visualization. This research method has been successfully applied in previous studies [4, 43]. The sooty flame strength is evaluated by the sooty radiation luminosity ratio (SLR). The relevant calculation formula is

$$\begin{aligned} \text{SLR} &= \sum R_{hue} \times \frac{\text{Sooty flame region}}{\text{Whole flame region}}, hue \in [0^\circ, 70^\circ] \\ &= \sum R_{hue} \times \frac{\text{Pixel No. of sooty flame}}{\text{Pixel No. of Whole flame area}}, hue \in [0^\circ, 70^\circ] \end{aligned} \quad \text{Equation 1}$$

where, the R is the intensity of the red tunnel in Red Green Blue (RGB) color mode. In this equation, only the R intensity in the Hue mode range from 0° to 70° is the effective calculation data for calculation, which is the soot-induced coloration. The sooty flame region has been divided into the overall flame area in advance. The dimensionless area calculation is based on the number of occupied pixels.

RESULTS AND DISCUSSION

In this section, the sooting propensity of different aromatic species and their proportion blends are demonstrated from two perspectives: PM emissions measured by DMS 500 and sooty flame morphology analyzed via the novel sooty flame imaging technique. The DMS 500 and imaging method were used for stable and LBO conditions, respectively. It has been found that DMS 500 has a limitation in measuring the emission profile at LBO. Hence, the image processing test method is used to evaluate emissions during LBO. The results were then found satisfactory and are discussed in details in the upcoming sections

Particulate Matter Emissions

It can be seen from Fig. 2 that, in general, as the mixing ratio increases, the PM emissions of all blended fuels show the increment. In particular, the increasing trend of indene series and naphthalene series blended fuels is relatively more significant, and the performance is more obvious in PM mass concentration.

Among the benzene series blended fuels, the emission of α -methylstyrene blended fuels is the highest in this group in terms of number concentration and mass concentration. On the contrary, 3-isopropyl cumene has the best emission performance in both aspects. . Except for these two types, there are emission differences among other types of aromatic hydrocarbon blending fuels, but there is no outstanding performance.

In the indene series, the indene and indane molecular structures are both a benzene ring plus a ring. Still, because the indene's molecular structure has one more bond than indane, it has a more stable molecular structure and is less likely to be decomposed and high PM emissions.

Tetrahydronaphthalene is obtained from hydrocracking of methyl naphthalene. And hence tetrahydronaphthalene does not possess a real naphthalene series aromatic structure (biphenyl ring). Moreover, after hydrotreating, the H/C ratio is increased by 32%, and the density is decreased by 3%. From the results of PM emission, it can be seen that the hydrotreated tetralin is significantly better than methyl naphthalene in terms of emissions and even lower than the emission performance of indene-based blended fuels. However, the specific energy per unit is increased by 1.855MJ/kg. Therefore, it can be seen that the hydrotreating of specific aromatics is an effective means to improve engine efficiency and reduce emissions.

The above discussion results show that the different molecular types and molecular structures of aromatic hydrocarbons have significant differences in the impact of fuel emissions. It also confirmed the importance of aromatic hydrocarbon content in particulate emissions and emphasized the necessity of controlling aromatic hydrocarbons to reduce particulate emissions from combustion. In addition, to a certain extent, it is proved that hydro processing is a crucial method to improve fuel quality.

From the results of PM quantity and mass concentration, it can be seen that when the volume fraction ratio of different aromatics is increased, the PM emission growth rate is different. Therefore, for the convenience of comparison, the calculated slope k analyzes the growth rate of PM emission after the linear fitting of each aromatic hydrocarbon growth line graph. The larger the k value, the faster the PM emission concentration increases with the volume fraction of fuel aromatics. The more incomplete the

combustion is, and vice versa. Record and sort the k of each growth line graph and draw it in Fig. 3.

It can be found from Fig. 3 that although the emission concentration of the blended fuels of cyclo-aromatic and di-aromatic is increased with the content of this type of aromatic hydrocarbon. However, the emission concentration growth rate is generally low, especially in terms of the emission quantity concentration growth. It is only 1/6 of the benzene series blended fuel, or less. Among them, the emission growth rate of tetralin blended fuel is the lowest. This also implicates that if due to actual combustion needs, such as achieving the required energy density, the content of aromatic hydrocarbons needs to be increased. Hence, the content of tetralin can be appropriately increased, and emissions can be effectively controlled simultaneously, thereby realizing the possibility of fuel performance optimization. In addition, although the overall emission base is low for benzene series, its growth rate is generally higher, especially for aromatic hydrocarbons such as diethyl benzene and trimethylbenzene. In other words, if such aromatic solvents are added to the fuel, the addition rate should be controlled to avoid exceeding the limit due to excessive emission growth. Finally, it is worth noting that for α -methylstyrene blended fuel, the increase in PM quantity and mass concentration is the slowest. In other words, if you continue to add this type of aromatic hydrocarbon, the fuel emissions will not change too much.

Relationship between characteristics and PM under stable combustion

Through previous literature surveys, it is found that the main characteristics that affect combustion emissions include density, molecular mass, carbon-to-hydrogen ratio,

molecular structure, etc. The influence of molecular structure on emissions and emission increase rate has been discussed in the previous section. In this section, we will analyze the relationship between other characteristics of aromatic hydrocarbons and PM emissions.

The linear regression algorithm is used to determine the linear relationship between aromatic hydrocarbons' characteristics and PM emission. The characteristics include density, molecular mass, hydrocarbon ratio, and specific energy, including four items. The different units and magnitudes of other characteristics make the calculated linear trend line gradient k to be horizontally comparable. The values of all characteristics in the x-axis direction are standardized in the range of 0 to 1, where 0 is the candidate fuel. The lowest value of the performance, 1 is the highest value, and the rest are scaled between 0-1. For example, the measured aromatic hydrocarbon's density range is 0.856-1.001, then 0 is 0.856, 1 is 1.001, and the remaining point's values are calculated according to Equation 2.

$$p_x^{0-1} = \frac{p_x - p_{min}}{p_{max} - p_{min}} \quad \text{Equation 2}$$

In the same way, the y-axis shows the standardized measurement of combustion PM emissions. The positive and negative values of the slope k can indicate the positive or negative influence of emissions' characteristic. A linear trend line is added to each graph, assuming linear regression for each set of data. The gradient of linear trend line is " k ", and the value of each is marked at the bottom of the graph. "Among them, the "-" symbol indicates that the combustion performance decreases with the increase of the fuel

property characteristic value. On the contrary, the "+" symbol indicates that the performance result has improved.

The calculation results and trends are shown in Fig. 4. It can be clearly seen from the figure that only the linear relationship between PM and hydrocarbon ratio in Fig. 4 (d) shows a downward trend, indicating that a high H/C ratio can effectively reduce Soot emissions. It is also worth noting that with the increase of aromatics content, the decline slope increased from 0.67 to 0.79, indicating that the higher the concentration of the aromatic, the more pronounced the improvement of PM emissions with the high H/C ratio. Conversely, the linear relationship between PM emission and density in Fig. 4(a) shows that when aromatic hydrocarbons have a high density, the fuel tends to emit higher PM emissions. Besides, as the concentration of aromatics increases, the slope k value increases from 0.74 to 0.87, and the degree of dispersion remains unchanged. On the same surface, as the aromatics concentration increases, density-induced PM emissions impact becomes more significant. Besides, for the other two characteristics, molecular mass, and specific energy, the point distribution is relatively discrete. The trend line does not increase or decrease significantly, indicating no direct linear relationship between these two characteristics and PM emissions.

Sooty flame profile at LBO condition

The sooty flame profile was also taken at LBO conditions, and a sequence of five consecutive images for different blends at 0.05s directly before blow-out are presented in Fig. 5. The details of the dynamic flame can be seen in the available video at the blow-out point [47]. As shown in the images, even in an extreme lean combustion condition,

the flame still exhibits varying degrees of a sooty flame appearance. The sooting propensity is dependent on the aromatics species and their proportion in fuels or fuel blends. The flame of heated soot particles is the cause of color emergence in the sooty flame region, as described earlier. Therefore, at LBO conditions, soot emissions can be indicated by the sooty flame area ratio. The blue flame and sooty flame of the images taken were filtered from 180° - 252° and 10° - 70° , respectively [48] within the hue value band (see Fig. 6). MATLAB was used to calculate the sooty flame area ratio.

Sooty flame morphology was more quantified through digital image processing by integrating the power spectrum for soot radiation concentration. The time resolved-dynamic properties of emitted soot radiation can be estimated by integrating relative R intensity through consecutive images taken by a high-speed camera. The time-domain image data was used to assess the spectrum and density amplitude through the PSD application. For the three sample aromatics blends at the same proportion of 13%, the soot radiation power amplitudes are in a variety of frequency spectrums, plotted in Fig. 7. As shown from the results, the dominant soot power density was distributed in the frequency range from 0 to 100 Hz approximately, and amplitude varied between different aromatics species. The soot radiation power amplitude of methylnaphthalene was notably higher than for the other two. The soot radiation power for all the tested blends is provided by integrating the energy-containing spectra for ease in comparison. Figure 8 shows the RMS of the power spectrum density of soot radiation power (SRP) for all 16 aromatic blends, at three proportions by volume and a stable operating condition. In all cases, the aromatic proportion increment promoted soot radiation strength.

Methynaphthalene had the worst performance and has the highest soot formation tendency during combustion, followed by species in the cyclo-aromatics group, particularly at the high proportion condition. The majority of alkyl-benzenes types of aromatics had lower soot radiation power, particularly for 3-Isopropylcumene. However, there was a sharp increase in the power amplitude for α -Methylstyrene and Pseudocumene blends at a high proportion, which is even higher than that of Tetrahydronaphthalene (cyclo-aromatic). As indicated in Fig. 8, RMS of the soot radiation power is decreasing with the rise of H/C ratio. All the alkyl-benzene blends generated relatively low soot radiation power and no apparent differences were found between species. The p-Cymene, tert-Butylbenzene, and 3-Isopropylcumene showed the lowest emissions due to their favorable physic-chemical properties (lower autoignition temperatures, lower boiling point, higher energy contents, etc.).

In contrast, the number concentration for α -Methylstyrene and diethyl benzene blends were slightly higher than the other candidate blends in the same chemical structure group. These outcomes are in good accordance with the other available literature on the same topic [45, 46]. The results revealed the impact of aromatic content on emissions and emphasized the significance of aromatic selection for lower emissions due to combustion.

PM emissions in CI engine

The experiment in the aviation combustor indicated that different aromatic species would produce different intensities of PM emission. The common thought of this phenomenon is due to different combustion environment such as pressure, injection

method. However, it is still unknown whether different aromatic species will affect PM results. These 16 aromatic species were tested in a CI (compression ignition) engine test rig.

The CI engine is a single cylinder direct injection method water-cooled [49]. Aromatics were blended with bannersol in a ratio of 31.5:1. The testing was done at a constant speed of 1500rpm and 5kw load. Instead of DMS 500, Laser-Induced Incandescence LII is selected in this test. The principle of LII is quite simple and reliable; exhaust entered into the LII through a heated sample line, a short high energy laser beam will hit the exhaust. According to the black body theory, any particles in exhaust absorb the energy and emit radiation. A series of photodetectors detect the thermal signal and transfer it into particle mass concentration via analysis. The results indicated that the CI engine produces higher PM number concentration (see Fig. 9). This due to the higher pressure and aromatic intensity in the combustor and fuel blend. The PM trend is quite interesting through each aromatic species in two test rig is similar to each other. Cyclo-aromatic and di- aromatic produce higher PM emissions than other aromatics, obviously in both two rigs, which means other than combustion conditions, aromatic species significantly affected PM production.

Comprehensive assessment

Since the primary purpose of adding aromatic hydrocarbons to aviation fuel is to ensure sufficient energy density, reducing emissions cannot be the only criterion for measuring the quality of aromatic hydrocarbons. Therefore, a comprehensive assessment of aromatics should be carried out. For this reason, this section will comprehensively

consider six aspects of fuel specific energy, PM emissions (quantity concentration/mass concentration), PM emission growth rate (quantity concentration/mass concentration), and sooty radiation power. Then it will calculate the comprehensive score after weighting it. Specifically, specific energy accounts for 50% of the evaluation factors, and all PM emission performance accounts for 50%. The specific distribution is shown in Table 3. The performance of 16 aromatic hydrocarbons is ranked, the highest specific energy is 1, and the lowest is 16. The lowest PM emission is 1, and the highest PM emission is 16. Each item's corresponding ranking is multiplied by the weight value and then added to obtain the final comprehensive ranking score. The specific calculation is shown in formula (2). The lowest score is the best aromatics, ranking first.

Comprehensive rank

$$\begin{aligned} &= n_{\text{specific energy}} \times 50\% + n_{PM\ No.} \times 20\% + n_{PM\ mas} \times 20\% \\ &+ n_{PM\ No.k} \times 10\% + n_{PM\ mss\ k} \times 10\% + n_{LBO\ sooty} \times 10\% \end{aligned} \quad \text{Equation 3}$$

The results of the comprehensive ranking are shown in the rightmost column of Table 2. Since the specific energy values of tert-butylbenzene, 3-isopropyl cumene and tert-butyl m-xylene have not been determined, it is necessary to set the average number for ranking temporarily, and the rankings are all 6. After considering energy density and emission factors, 3-isopropyl cumene ranked first, mainly due to its low emissions. Still, because its specific energy value is unknown, it is only for reference and not the final result. If its specific energy can reach above the average value, it can become the best aromatics choice. Cumene and Diethylbenzene have a mid-to-high performance in all

aspects of specific energy and emissions, and their overall strength is relatively good, ranking second and third, respectively.

On the contrary, trimethylbenzene, α -methylstyrene, and methylnaphthalene ranked the bottom three. Although toluene and α -methylstyrene are benzene series, their performance is the worst in the benzene series, and their specific energy is also low. Methylnaphthalene fuelled combustion system emitted higher pollutants due to their higher degree of unsaturation and poor specific energy, and hence ranks last [50, 51]. However, tetralin's overall performance is significantly improved in terms of specific energy and finally ranked in the middle. It can be seen that hydroprocessing can effectively reduce emissions and increase specific energy, which is of great significance to fuel optimization [52].

CONCLUSION

This study conducted systematic experiments and analysis on the impact of 16 aromatic blended fuels on PM emissions. The research results have guiding significance for optimizing aviation fuel with low carbon smoke emission and the development of alternative fuels. The result shows:

- The different molecular types and molecular structures of aromatic hydrocarbons have significant differences in fuel emissions. Controlling the types of aromatic hydrocarbons can be an effective means to reduce particulate emissions from combustion.
- The emission concentration of the blended fuel of indene and naphthalene is very high. When its content is increased, the emission concentration growth rate is

much lower than that of benzene. When the content of α -methylstyrene blended fuel in the benzene series increases, the number of emitted particles does not change much, but individual particles mass increases significantly.

- The molecular structure plays a crucial role in emissions. Besides, high density is another important factor leading to the formation of soot. The high H/C ratio has an excellent inhibitory effect on soot formation.
- Cumene and styrene have the best overall performance in terms of emissions and specific energy. Besides, hydroprocessing can reduce emissions while increasing specific energy, which is an effective means to optimize fuel's overall performance.
- Different aromatic species on PM emissions in CI engine and aviation combustor have a similar trend. Overall, the alkyl-benzene category of aromatics showed the best performance related to lower soot-formation tendency. Additionally, it was observed that di-aromatics and cyclo-aromatics produced significantly higher soot emissions compared to alkyl-benzenes. Therefore, it can be deduced that the molecular chemical structure of the aromatics shows a key role in soot emission.
- Methylnaphthalene from the di-aromatics category had the worst impact on all PM and SRP evaluations at LBO, particularly at high proportions. On the other hand, 3-Isopropylcumene blends had the lowest emission rate and SRP. The blends with toluene and o-Xylene exhibit the smallest sooty area ratio and the increase rate was relatively low. This indicates that they offer the best performance for promoting sufficient burning

and low emission. There is a possibility of tuning the aromatic type in future fuels to achieve lower emissions and better systems compatibility

Acknowledgement

This work has been supported by University of Sheffield's Low Carbon Combustion Centre. Part of this work was supported by the Nanjing Institute of Technology Research start-up Project (grant number YKJ201902), Jiangsu Education Department General Program (grant number 19KJB590002).

Supplementary information

The experimental data would be provided on individual request basis for future studies.

Accepted Manuscript Not Copyable

REFERENCES

- [1] Feser, J., and Gupta, A.K., 2020 "Performance and Emissions of Drop-In Aviation Biofuels in a Lab-Scale Gas Turbine Combustor." ASME. *J. Energy Resour. Technol.* April 2021; 143(4): 042103. <https://doi.org/10.1115/1.4048243>
- [2] Turkyilmazoglu, M., 2020. Combustion of a solid fuel material at motion. *Energy*, p.117837.
- [3] Ubogu, E. A., Cronly, J., Khandelwal, B., and Roy, S. 2018, "Determination of the effective density and fractal dimension of PM emissions from an aircraft auxiliary power unit." *J. of Environmental Sciences china*, Vol. 74, pp. 11-18, doi: 10.1016/j.jes.2018.01.027
- [4] Zheng, L., Ling C., Ubogu, E.A., Cronly, J., Ahmed, I., Zhang, Y., Khandelwal, B., 2018, "Effects of Alternative Fuel Properties on Particulate Matter Produced in a Gas Turbine Combustor" *Energy & Fuels*, Vol. 32, No. 9, , pp.9883-9897. doi: 10.1021/acs.energyfuels.8b01442
- [5] Sadiq, A.M., Sleiti, A.K. and Ahmed, S.F., 2020. Turbulent Flames in Enclosed Combustion Chambers: Characteristics and Visualization—A Review. *Journal of Energy Resources Technology*, 142(8)
- [6] Siegmann, .K., Sattler, K., Siegmann, H.C., 2002, "Clustering at high temperatures: carbon formation in combustion," *J. of Electron Spectroscopy and Related Phenomena*, Vol. 126, No. 1, 2002, pp. 191–202. doi: 10.1016/S0368-2048(02)00152-4
- [7] McEnally, C. S., Pfefferle, L. D., Atakan, B., Kohse-Höinghaus, K., 2006, "Studies of aromatic hydrocarbon formation mechanisms in flames: Progress towards closing the fuel gap," *Progress in Energy and Combustion Science*. Vol. 32, pp. 247–294. doi: 10.1016/j.pecs.2005.11.003
- [8] Chen, D., Zainuddin. Z., Yapp, E., Akroyd, J., Mosbach, S., Kraft, K., "A fully coupled simulation of PAH and soot growth with a population balance model," *Proc. Combust. Inst.* Vol. 34, 2013, pp. 1827–1835. doi: 10.1016/j.proci.2012.06.089
- [9] Saffaripour, M., Zabeti, P., Kholghy, M., Thomson, M. J., "An experimental comparison of the sooting behavior of synthetic jet fuels," *Energy and Fuels*. Vol. 25, 2011, pp. 5584–5593. doi:10.1021/ef201219v.

- [10] Braun-Unkhoff, M., Kathrotia, T., Rauch, B., Riedel, U., "About the interaction between composition and performance of alternative jet fuels," *CEAS Aeronaut. J.* Vol. 7, 2016, pp. 83–94. doi:10.1007/s13272-015-0178-8.
- [11] Singh, A. P., Bajpai, N., and Agarwal, A. K., 2018, "Combustion Mode Switching Characteristics of a Medium-Duty Engine Operated in Compression Ignition/PCCI Combustion Modes." *ASME. J. Energy Resour. Technol.* Vol. 140(9), pp. 092201. <https://doi.org/10.1115/1.4039741>
- [12] Lobo, P., Christie, S., Khandelwal, B., Blakey, S.G., Raper, D.W., "Evaluation of Non-volatile Particulate Matter Emission Characteristics of an Aircraft Auxiliary Power Unit with Varying Alternative Jet Fuel Blend Ratios," *Energy and Fuels.* Vol. 29, 2015, pp. 7705–7711. doi: 10.1021/acs.energyfuels.5b01758.
- [13] Silverman, B., "Effects of High Aromatic Aviation Fuel on Sealant Systems," 1980. doi:10.4271/800881.
- [14] Chen, K., Liu, H., Xia, Z., "The Impacts of Aromatic Contents in Aviation Jet Fuel on the Volume Swell of the Aircraft Fuel Tank Sealants," *SAE Int. J. Aerosp.* Vol. 6, 2013 doi:10.4271/2013-01-9001.
- [15] Khandelwal, B., Roy, S., Lord, C., Blakey, S., "Comparison of vibrations and emissions of conventional jet fuel with stressed 100% SPK and fully formulated synthetic jet fuel," *Aerospace.* Vol.1, 2014, pp. 52–66. doi: 10.3390/aerospace1020052
- [16] ASTM D7655-12, "Standard Specification for Aviation Turbine Fuel Containing Synthesized Hydrocarbons BT - Standard Specification for Aviation Turbine Fuel Containing Synthesized Hydrocarbons," *ASTM International, West Conshohocken, PA*, 2019, doi: 10.1520/D7566-12
- [17] Ruslan, M., Ahmed, I., Khandelwal, B., "Evaluating Effects of Fuel Properties on Smoke Emissions," 2016, doi: 10.1115/GT2016-56791.
- [18] Duvvuri, P. P., Sukumaran, S., Shrivastava, R. K., and Sreedhara, S., 2019, "Modeling the Effect of Parametric Variations on Soot Particle Size Distribution in a Diesel Engine." *ASME. J. Energy Resour. Technol.* Vol. 142(3), pp. 032201. <https://doi.org/10.1115/1.4044563>
- [19] Lim, S., Ahn, T., Lee, S., Park, S., "Optical measurement of volume fraction and organic mass fraction of ultra-fine soot particles emitted from inverse

- diffusion flames," *Fuel*. Vol. 210, 2017, pp. 455–462. doi:10.1016/j.fuel.2017.08.113.
- [20] Scenna, R., and Gupta, A. K., 2018 "The Influence of the Distributed Reaction Regime on Fuel Reforming Conditions." *ASME. J. Energy Resour. Technol.* Vol. 140(12), pp. 122002. <https://doi.org/10.1115/1.4040404>
- [21] Balakrishnan, A., Parthasarathy, R. N., and Gollahalli, S. R., 2015, "Combustion Characteristics of Partially Premixed Prevaporized Palm Methyl Ester and Jet A Fuel Blends." *ASME. J. Energy Resour. Technol.* vol. 138(1), pp. 012202. <https://doi.org/10.1115/1.4031966>
- [22] Kitsopanidis, I., Cheng, W. K., "Soot Formation Study in a Rapid Compression Machine," *J. Eng. Gas Turbines Power*. Vol. 128, 2006, pp. 942. doi:10.1115/1.2180279.
- [23] Scenna, R., and Gupta, A. K., 2015, "Preheats Effects on JP8 Reforming Under Volume Distributed Reaction Conditions." *ASME. J. Energy Resour. Technol.* Vol. 138(3), pp. 032202. <https://doi.org/10.1115/1.4032140>
- [24] Lobo, P., Durdina, L., Smallwood, G. J., Rindlisbacher, T., Siegerist, F., Black, E. A., Yu, Z., Mensah, A. A., Hagen, D. E., Miake-Lye, R. C., Thomson, K. A., Brem, B. T., Corbin, J. C., Abegglen, M., Sierau, B., Whitefield, P. D., Wang, J., "Measurement of aircraft engine non-volatile PM emissions: Results of the Aviation-Particle Regulatory Instrumentation Demonstration Experiment (A-PRIDE) 4 campaign," *Aerosol Sci. Technol.* Vol. 49, 2015 pp. 472–484. doi:10.1080/02786826.2015.1047012.
- [25] Krabicka, J., Lu, G., "Visualisation and Characterisation of Flame Radical Emissions through Intensified Spectroscopic Imaging," Vol. 178, 2009, pp. 1–5. doi:10.1088/1742-6596/178/1/012041.
- [26] Kim, W., Sivathanu, Y., Gore, J. P., "Characterization of spectral radiation intensities from standard test fires for fire detection," *NIST Spec. Publ. SP.* 2001, pp. 91–106.
- [27] Bäckström, D., Gunnarsson, A., Gall, D., Pei, X., Johansson, P., Andersson, K., Pathak, R. K. Pettersson, J. B. C., "Measurement of the size distribution, volume fraction and optical properties of soot in an 80 kW propane flame," *Combust. Flame*. Vol. 186, 2017, pp. 325–334. doi: 10.1016/j.combustflame.2017.08.023.

- [28] Botero, M. L., Mosbach, S., Kraft, M., "Sooting tendency and particle size distributions of n-heptane/toluene mixtures burned in a wick-fed diffusion flame," *Fuel*. Vol. 169, 2016, pp. 111–119. doi: 10.1016/j.fuel.2015.12.014.
- [29] Fujino, R., Aoyagi, Y., Osada, H., Yamaguchi, T., Mizuno, S., "Direct Observation of Clean Diesel Combustion using a Bore Scope in a Single Cylinder HDDE," 2009. doi: 10.4271/2009-01-0645
- [30] Jiotode, Y., Agarwal, A. K., "Endoscopic Combustion Visualization for Spatial Distribution of Soot and Flame Temperature in a Diesohol Fueled Compression Ignition Engine," *Energy and Fuels*. Vol. 30, 2016 pp. 9850–9858. doi:10.1021/acs.energyfuels.6b01585.
- [31] Botero, M. L., Mosbach, S., Kraft, M., "Sooting tendency of paraffin components of diesel and gasoline in diffusion flames," *Fuel*. Vol. 126, 2014, pp. 8–15. doi: 10.1016/j.fuel.2014.02.005.
- [32] Botero, M. L., Mosbach, S., Akroyd, J., Kraft, M., "Sooting tendency of surrogates for the aromatic fractions of diesel and gasoline in a wick-fed diffusion flame," *Fuel*. Vol. 153, 2015, pp. 31–39. doi: 10.1016/j.fuel.2015.02.108.
- [33] Witkowski, D., Kondo, K., Vishwanathan, G., Rothame, D., "Evaluation of the sooting properties of real fuels and their commonly used surrogates in a laminar co-flow diffusion flame," *Combust. Flame*. Vol. 160, 2013, pp. 1129–1141. doi:10.1016/j.combustflame.2013.01.027.
- [34] Huang, H., Zhang, Y., "Flame colour characterization in the visible and infrared spectrum using a digital camera and image processing," *Measurement Science and Technology*, Vol.19, 2018 doi:10.1088/0957-0233/19/8/085406.
- [35] Huang, H. W., Zhang, Y., "Digital colour image processing based measurement of premixed CH₄ + air and C₂H₄ + air flame chemiluminescence," *Fuel*. Vol. 90, 2011, pp. 48–53. doi:10.1016/j.fuel.2010.07.050.
- [36] Ng, W. B., Clough, E., Syed, K. J., Zhang, Y., "The combined investigation of the flame dynamics of an industrial gas turbine combustor using high-speed imaging and an optically integrated data collection method," *Meas. Sci. Technol.* Vol. 15, 2004 pp. 2303–2309. doi:10.1088/0957-0233/15/11/016.
- [37] Zheng, L. Faik, A., Zhang, Y., "Flame colour analysis for the droplet combustion of water-in-diesel emulsions," *12th Int. Conf. Heat Transf. Fluid Mech.*

*Thermodyn., Malaga, Spain, 2016: pp. 212–217. URL:
<https://edas.info/web/hefat2016/titles.html#F>.*

- [38] Symonds, J. P. R., Reavell, K. S. J., Olfert, J. S., Campbell, B. W., Swift, S. J., “Diesel soot mass calculation in real-time with a differential mobility spectrometer,” *J. Aerosol Sci.* Vol.38, 2007, pp. 52–68.
- [39] Rye, L., Lobo, P., Williams, P.I., Uryga-Bugajska, I., Christie, S., Wilson, C., Hagen, D., Whitefield, P., Blakey, S., Coe, H., Raper, D., Pourkashanian, M., “Inadequacy of optical smoke measurements for characterization of non-light absorbing particulate matter emissions from gas turbine engines,” *Combust. Sci. Technol.* Vol. 184, 2012, pp. 2068–2083. doi:10.1080/00102202.2012.697499.
- [40] Petzold, A., Marsh, R., Johnson, M., Miller, M., Sevcenco, Y., Delhay, D., Ibrahim, A., Williams, P., Bauer, H., Crayford, A., Bachalo, W. D., Raper, D., “Evaluation of Methods for Measuring Particulate Matter Emissions from Gas Turbines,” *Environ. Sci. Technol.* Vol. 45, 2011 pp. 3562–3568. doi:10.1021/es103969v.
- [41] McKerrell, E. H., “Determination of aromatic hydrocarbon types in diesel fuels: An assessment of method IP391/90 and a proposed modification,” *Fuel.* Vol. 72, 1993, pp. 1403–1409. doi: 10.1016/0016-2361(93)90416-Y
- [42] Rye, L., Wilson, C., “The influence of alternative fuel composition on gas turbine ignition performance,” *Fuel.* Vol. 96, 2012, pp. 277–283. doi: 10.1016/j.fuel.2011.12.047.
- [43] Zheng, L., Cronly J, Emamode Ubogu, Ihab Ahmed, Yang Zhang, Khandelwal, B. 2019, "Experimental investigation on alternative fuel combustion performance using a gas turbine combustor", *Applied Energy*, Vol. 238, pp. 1530-1542.
- [44] Zheng, L., Zhang, Y., “High Speed Digital Imaging for Flame Studies: Potentials and Limitations, in: *Energy Procedia*,” Elsevier Ltd, 2015, pp. 237–240.
- [45] DeWitt, M. J., Corporan, E., Graham, J., Minus, D., “Effects of aromatic type and concentration in Fischer-Tropsch fuel on emissions production and material compatibility,” *Energy and Fuels.* Vol. 22, 2008, pp. 2411–2418. doi:10.1021/ef8001179.

- [46] Khandelwal, B., Cronly, J., Ahmed, I. S., Wijesinghe, C. J., Lewis. C., "The effect of alternative fuels on gaseous and particulate matter (PM) emission performance in an auxiliary power unit (APU)." *The Aeronautical Journal*, 2019, pp. 1–19. doi: 10.1017/aer.2019.16
- [47] Lukai Zheng, "Flame visualization of Toluene, Indene and Methyl-naphthalene blending with base solvent at LBO," 2018. <https://youtu.be/XOp1FZOdhTI>.
- [48] Wang, Y., Zheng, L., Woolley, R., Zhang, Y., "Investigation of ignition process from visible to infrared by a high speed colour camera," *Fuel*. Vol. 185, 2016 doi:10.1016/j.fuel.2016.08.010.
- [49] Almohammadi, B.A., Singh, P., Sharma, S., Kumar, S. and Khandelwal, B., 2020. "Impact of alkylbenzenes in formulated surrogate fuel on characteristics of compression ignition engine". *Fuel*, 266, p.116981. <https://doi.org/10.1016/j.fuel.2019.116981>
- [50] Singh, P., Sharma, S., Almohammadi, B.A., Khandelwal, B. and Kumar, S., 2020. "Applicability of aromatic selection towards newer formulated fuels for regulated and unregulated emissions reduction in CI engine". *Fuel Processing Technology*, 209, p.106548. <https://doi.org/10.1016/j.fuproc.2020.106548>
- [51] Sharma, S., Singh, P., Almohammadi, B.A., Khandelwal, B. and Kumar, S., 2020. "Testing of formulated fuel with variable aromatic type and contents in a compression-ignition engine". *Fuel Processing Technology*, 208, p.106413. <https://doi.org/10.1016/j.fuproc.2020.106413>
- [52] Kumar, N., Sonthalia, A. and Koul, R., 2020. Optimization of the process parameters for hydrotreating used cooking oil by the Taguchi method and Fuzzy logic. *Journal of Energy Resources Technology*, pp.1-41.

Figure Captions List

- Fig. 1 Testing set up with the Tay combustor [42]
- Fig. 2 PM particle quantity and quality results of 16 kinds of aromatic hydrocarbons and 3 kinds of ratio mixed fuel
- Fig. 3 The growth rate of PM of 16 aromatic hydrocarbon mixed fuels
- Fig. 4 Linear relationship between aromatic hydrocarbon characteristics and PM emission; (a) PM vs Density; (b) PM vs molecular weight; (c) PM vs Specific energy; (d) PM vs H/C ratio.
- Fig. 5 Sample images of indene in proportions of 8%, 13%, and 18% during the final 0.05s before LBO point
- Fig. 6 Power spectrum density of the blended fuel with 13% toluene (alkyl-benzenes), indene (cyclo-aromatics) and methylnaphthalene (di-aromatics)
- Fig. 7 Sooty flame area ratio for 16 types of aromatics blends, with three proportions by volume at LBO condition
- Fig. 8 Effect of H/C ration in sooty flame radiation power
- Fig. 9 Effect of aromatic species on PM mass concentration in two test rigs

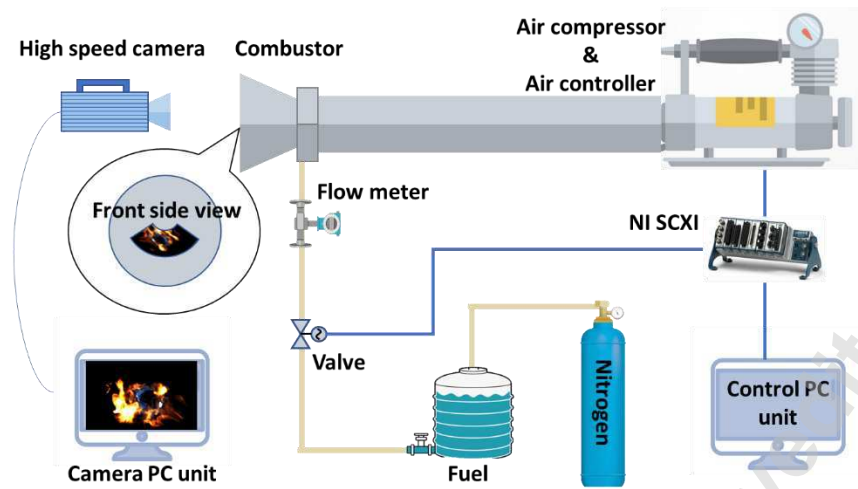


Fig. 1. Testing set up with the Tay combustor [42]

Accepted Manuscript Not Certified

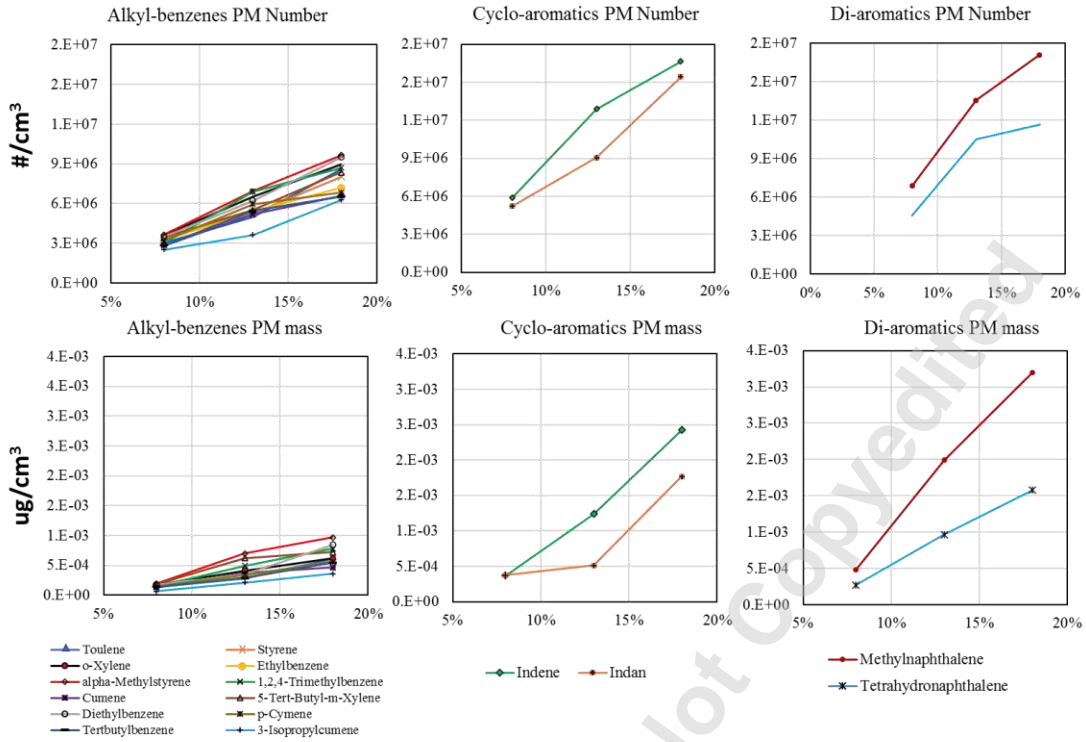


Fig. 2. PM particle quantity and quality results of 16 kinds of aromatic hydrocarbons and 3 kinds of ratio mixed fuel
 (The details of the data are shown in Appendix I)

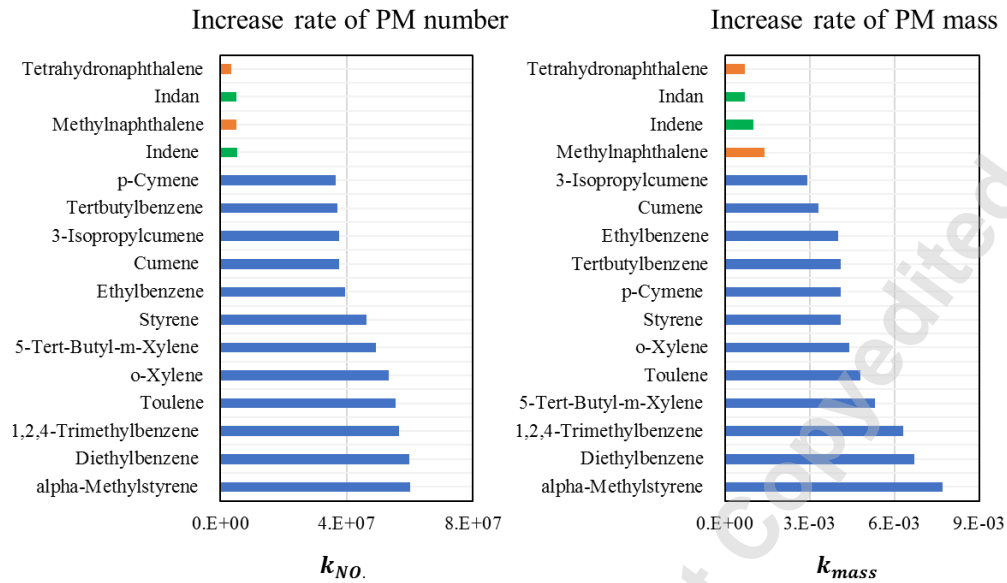


Fig. 3. The growth rate of PM of 16 aromatic hydrocarbon mixed fuels

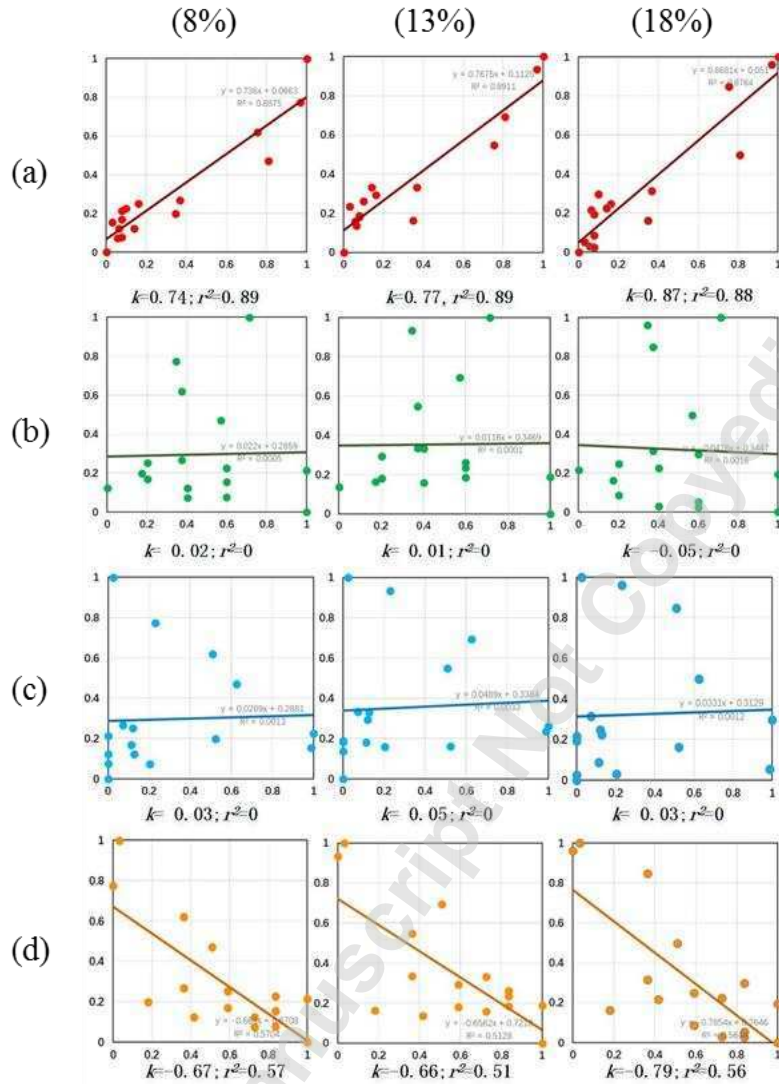


Fig. 4. Linear relationship between aromatic hydrocarbon characteristics and PM emission; (a) PM vs Density; (b) PM vs molecular weight; (c) PM vs Specific energy; (d) PM vs H/C ratio

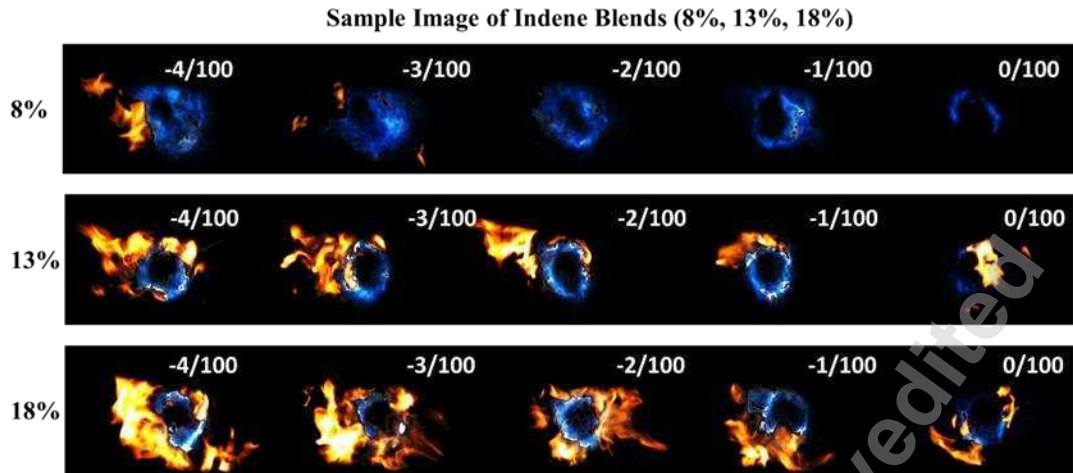


Fig. 5. Sample images of indene in proportions of 8%, 13%, and 18% during the final 0.05s before LBO point

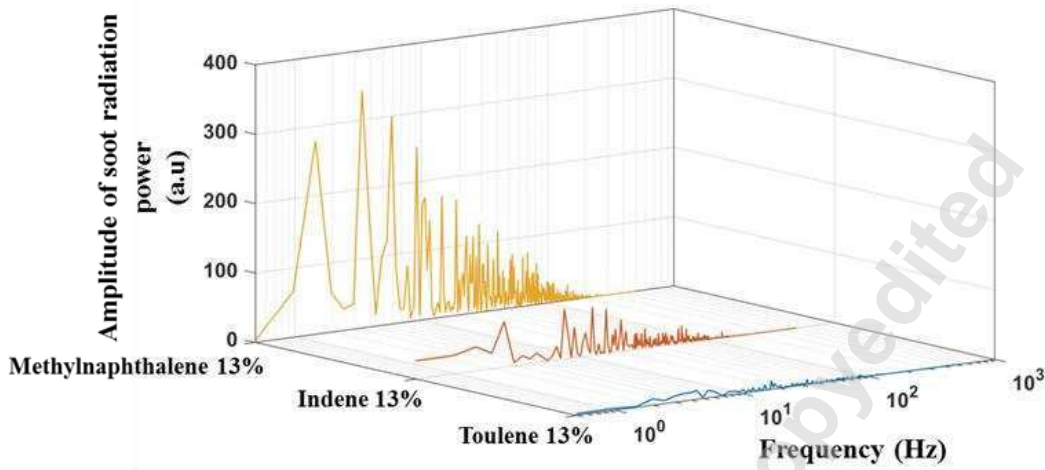


Fig. 6. Power spectrum density of the blended fuel with 13% toluene (alkyl-benzenes), indene (cyclo-aromatics) and methylnaphthalene (di-aromatics)

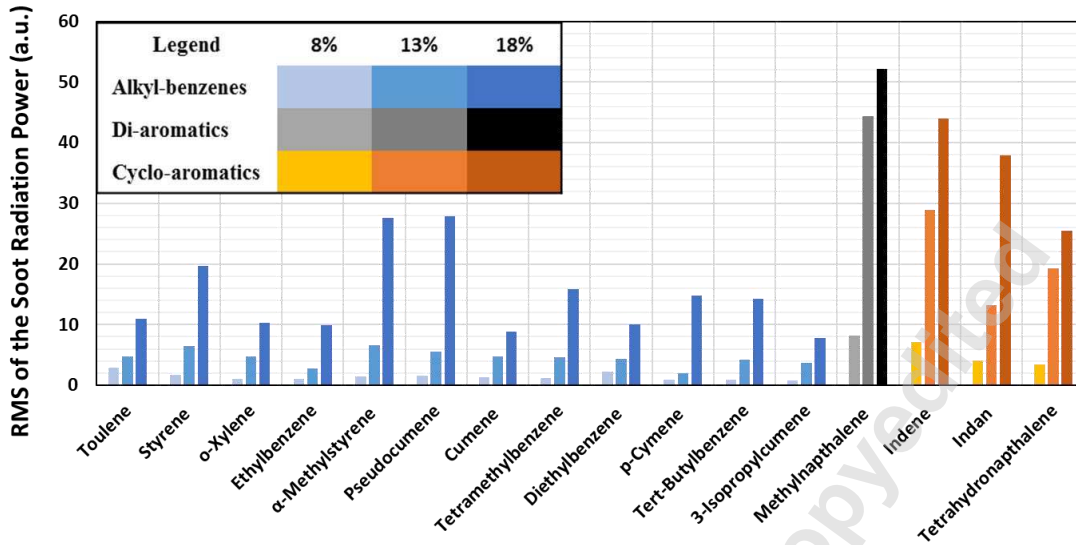


Fig. 7. Sooty flame area ratio for 16 types of aromatics blends, with three proportions by volume at LBO condition

Accepted Manuscript Not Copyable

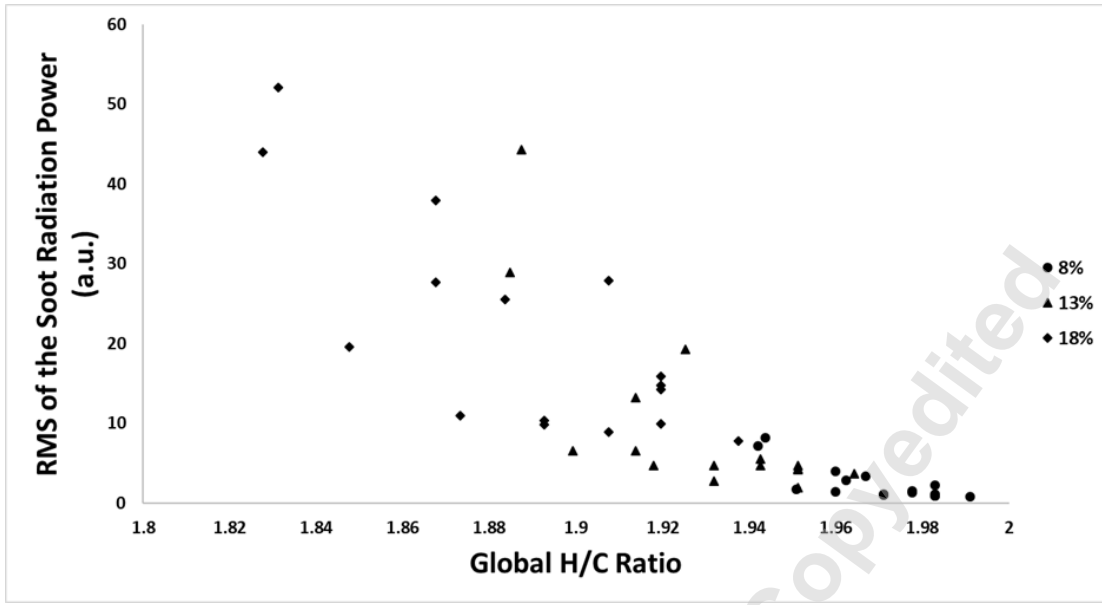


Fig. 8. Effect of H/C ration in sooty flame radiation power

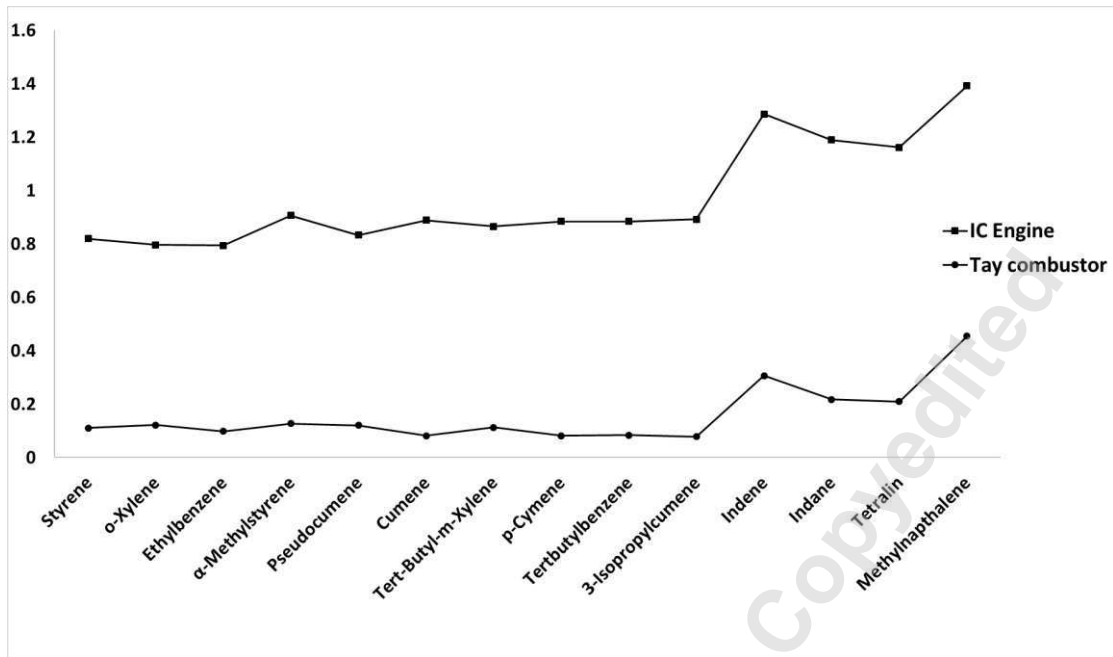


Fig. 9. Effect of aromatic species on PM mass concentration in two test rigs

Table Caption List

| | |
|---------|--|
| Table 1 | Candidate aromatics species |
| Table 2 | Testing parameters for the LBO and stable conditions |
| Table 3 | Performance ranking and weight allocation and comprehensive ranking of 16 aromatic hydrocarbons |

Accepted Manuscript Not Copyedited

Table 1. Candidate aromatics species

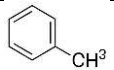
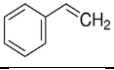
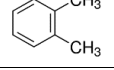
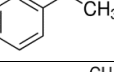
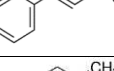
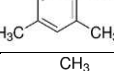
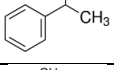
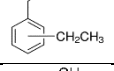
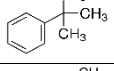
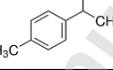
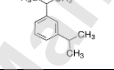
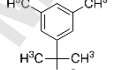
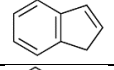
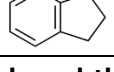
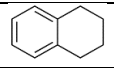
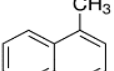
| Name | Structure | Density [gcm-3] | Specific Energy [MJ/kg] | Molecular Mass [g/mol] | H/C Ratio |
|--|---|-----------------|-------------------------|------------------------|-----------|
| Alky-benzenes | | | | | |
| Toluene |  | 0.865 | 40.589 | 92.14 | 1.143 |
| Styrene |  | 0.906 | 42.205* | 104.15 | 1.000 |
| o-Xylene |  | 0.879 | 40.961 | 106.17 | 1.250 |
| Ethylbenzene |  | 0.867 | 40.938 | 106.17 | 1.250 |
| α -Methylstyrene |  | 0.909 | 40.810 | 118.18 | 1.111 |
| Pseudocumene |  | 0.876 | 40.984 | 120.19 | 1.333 |
| Cumene |  | 0.864 | 41.217 | 120.19 | 1.333 |
| Diethylbenzene |  | 0.87 | 43.683f | 134.22 | 1.4 |
| Tert-butylbenzene |  | 0.867 | --- | 134.22 | 1.4 |
| p-Cumene |  | 0.86 | 43.644 | 134.22 | 1.4 |
| 3-isopropyl cumene |  | 0.856 | --- | 162.27 | 1.5 |
| Tert-butyl m-xylene |  | 0.867 | --- | 162.27 | 1.5 |
| Cycl-aromatics | | | | | |
| Indene |  | 0.996 | 41.300 | 116.16 | 0.889 |
| Indane |  | 0.965 | 42.162 | 118.176 | 1.111 |
| Alkyl-naphthalene (Di-aromatic) | | | | | |
| Tetralin |  | 0.973 | 42.523 | 132.2 | 1.2 |
| Methylnaphthalene |  | 1.001 | 40.668 | 142.2 | 0.909 |

Table 2. Testing parameters for the LBO and stable conditions

| Condition | Atomization pressure (kPa) | Fuel pressure (kPa) | Air-mass flow (kg/s) | Fuel flow rate (g/s) |
|------------------|---------------------------------------|--------------------------------|---------------------------------|---------------------------------|
| LBO | 40 | 150 | 0.2 | Real time |
| Stable | 80 | 300 | 0.2 | 1.8 |

Accepted Manuscript Not Copyedited

Table 3. Performance ranking and weight allocation and comprehensive ranking of 16 aromatic hydrocarbons

| | Specific Energy | PM number | PM mass | $k_{No.}$ | k_{mass} | soot radiation power | Total | Rank |
|-------------------------|-----------------|-----------|---------|-----------|------------|----------------------|-------|------|
| | 50% | 10% | 10% | 10% | 10% | 10% | | |
| 3-isopropyl cumene | 6 | 1 | 1 | 3 | 5 | 6 | 4.6 | 1 |
| p-Cumene | 2 | 5 | 7 | 10 | 9 | 5 | 4.6 | 2 |
| Diethylbenzene | 1 | 11 | 9 | 2 | 15 | 7 | 4.9 | 3 |
| Styrene | 4 | 6 | 5 | 9 | 10 | 4 | 5.4 | 4 |
| Tetrahydronaphthalene | 3 | 13 | 14 | 11 | 1 | 14 | 6.8 | 5 |
| Tert-butylbenzene | 6 | 3 | 3 | 16 | 8 | 12 | 7.2 | 6 |
| Tert-butyl m-xylene | 6 | 8 | 11 | 6 | 13 | 8 | 7.6 | 7 |
| Cumene | 10 | 2 | 2 | 12 | 6 | 9 | 8.1 | 8 |
| Indan | 5 | 14 | 13 | 15 | 2 | 13 | 8.2 | 9 |
| Ethylbenzene | 13 | 4 | 4 | 1 | 7 | 3 | 8.4 | 10 |
| O-xylene | 12 | 10 | 8 | 4 | 11 | 2 | 9.5 | 11 |
| Indene | 9 | 15 | 15 | 8 | 3 | 15 | 10.1 | 12 |
| Pseudocumene | 11 | 9 | 10 | 14 | 14 | 10 | 11.2 | 13 |
| Toluene | 16 | 7 | 6 | 7 | 12 | 1 | 11.3 | 14 |
| α -Methylstyrene | 14 | 12 | 12 | 5 | 16 | 11 | 12.6 | 15 |
| Methyl naphthalene | 15 | 16 | 16 | 13 | 4 | 16 | 14 | 16 |